Universiteit
Leiden
The Netherlands

Arabidopsis AGC3 kinases and PIN plasma membrane abundance

Gelderen, K. van

Citation
Gelderen, K. van. (2017, July 6). *Arabidopsis AGC3 kinases and PIN plasma membrane abundance*. Retrieved from https://hdl.handle.net/1887/50504

Version:	Not Applicable (or Unknown)
License:	Licence agreement concerning inclusion of doctoral thesis in the Institutional Repository of the University of Leiden
Downloaded from:	https://hdl.handle.net/1887/50504

Note: To cite this publication please use the final published version (if applicable).

Cover Page

Universiteit Leiden

The handle http://hdl.handle.net/1887/50504 holds various files of this Leiden University dissertation

Author: Gelderen, Kasper van
Title: Arabidopsis AGC3 kinases and PIN plasma membrane abundance
Issue Date: 2017-07-06

Chapter 6

PINOID and its homolog AGC3-4 modulate photomorphogenesis and PIN1 turnover through CSN and COP1

Kasper van Gelderen[1], Felipe dos Santos Maraschin[2], Marcelo Kemel-Zago, Rene Benjamins[3], Kiki Spaninks, Stef Janson[4], Stefan Elzinga, Anne Otten, Remko Offringa[#]

Plant developmental genetics, Institute of Biology, Leiden University,
Sylviusweg 72, 2333 BE Leiden, The Netherlands.
[1] Current affilication: Plant Ecophysiology, Institute of Environmental Biology, Utrecht University,
Padualaan 8, 3584 CH Utrecht, The Netherlands.
[2] Current affiliation: Universidade Federal do Rio Grande do Sul, Instituto de Biociências,
Departamento de Botânica. Bento Gonçalves 9500, Porto Alegre, 91501970, Brazil.
[3] Current affiliation: Syngenta seeds B.V., Westeinde 62 1601 BK Enkhuizen, The Netherlands.
[4] Current affiliation: Leiden University Medical Center, department of Molecular Cell Biology,
Einthovenweg 20, 2300 RC Leiden, The Netherlands.

Author for correspondence: r.offringa@biology.leidenuniv.nl

Abstract

When plant seedlings germinate, their cotyledons remain folded and protected by an apical hook, while the rapidly elongating hypocotyl pushes them through the soil toward the light. Once the seedling shoot reaches the light, the photomorphogenesis program is switched on, resulting in: loss of the apical hook, cotyledon opening, reduced hypocotyl elongation, initiation of chloroplast biogenesis and photosynthesis; which triggers root development. A central regulator in this process CONSTITUTIVE PHOTOMORPHOGENESIS 1 (COP1) acts downstream of the photoreceptors to repress photomorphogenesis-related gene expression and protein abundance. The PIN-FORMED (PIN) auxin efflux carriers are important downstream targets, as COP1 represses active auxin distribution by promoting vacuolar targeting of these transmembrane proteins. The mechanism by which COP1 acts on PIN plasma membrane (PM) abundance is not yet clear. Here we show that the AGC3 protein serine/threonine kinase PINOID (PID) that is well-known for directing PIN polarity by phosphorylating these auxin carriers at the PM, and its close homolog AGC3-4 can enhance PIN protein abundance through a novel nuclear function. PID is a PM-associated kinase and AGC3-4 localizes both to the PM and the nucleus. These kinases were found to interact with COP9 SIGNALOSOME SUBUNIT8 (CSN8) and COP1 and to phosphorylate COP1 and CNS7. For seedlings overexpressing PID (*35S::PID*) only hypocotyl length and apical hook formation was affected, but overexpression of nuclear PID (*35S::SV40-PID*) or AGC3-4 (*35S::AGC3-4*) resulted in more clear *cop1/csn*-like phenotypes, suggesting that the kinases repress COP1 and CSN function. Furthermore, *35S::SV40-PID* seedlings showed enhanced root growth in the dark, whereas root growth of dark grown *35S::PID* seedlings was decreased. These findings indicate that AGC3, PID(-like) kinases can function in the nucleus, separately from PIN proteins, and affect photomorphogenesis, possibly via repression of COP1.

Introduction

Seed plants generally grow with one half of their body in the dark soil and the other half in the light. However, they start their life in the dark soil as a seed and during germination the transition from dark growth (skotomorphogenesis) to light growth (photomorphogenesis) is a crucial moment for the establishment of a plant's life. This transition involves a reduction in hypocotyl elongation, apical hook opening and the start of photosynthesis, which subsequently triggers shoot and root development. In the dark, a specialized ubiquitin ligase complex containing the RING-E3-Ub-ligase CONSTITUTIVE PHOTOMORPHOGENESIS (COP1), induces the degradation of transcription factors that normally are associated with light growth, such as ELONGATED HYPOCOTYL 5 (HY5), HY5-HOMOLOG (HYH) and PHYTOCHROME INTERACTING FACTOR 1 (PIF1) (Lau and Deng, 2012; Zhu et al., 2015). The activity of COP1 is dependent on the binding of a family of cofactors called SUPPRESSOR OF PHYA-105 (SPA) (Laubinger et al., 2004). When light is perceived by the seedling, Phytochrome A (PhyA) and Phytochrome B (PhyB) bind to the SPA proteins and thereby deactivate COP1, causing photomorphogenic transcription factors to accumulate (Sheerin et al., 2015). COP1 activity is also modulated by the COP9-SIGNALOSOME (CSN), a multi-subunit protease-like complex that regulates the activity of CULLIN-RING (CUL) ligases, which aid COP1 among others in ubiquitinating targets (Lau and Deng, 2012) and can be found throughout the eukaryotic kingdom (Wei et al., 2008).

Root development of Arabidopsis depends on sugars and hormones produced in the shoot, and in dark-grown seedlings (without photosynthesis) root development is severely reduced (Kircher and Schopfer, 2012). Lateral root development in young seedlings can be stimulated by shoot-produced auxin (Bhalerao et al., 2002). Shoot-produced auxin is thought to be transported to the root via polar cell-to-cell transport driven by PIN-FORMED (PIN) auxin efflux carriers that are asymmetrically placed at the plasma membrane (PM) (Petrásek et al., 2006; Wisniewska et al., 2006). The direction of transport is determined by the polar subcellular localization of PIN proteins, and the AGC3 protein serine/threonine kinases PID, WAG1 and WAG2 have been shown to direct shootward PIN polarity and thus auxin transport by phosphorylating PIN proteins at conserved motifs in the their hydrophilic loop (Chapter 2) (Dhonukshe et al., 2010; Huang et al., 2010; Wisniewska et al., 2006). The capacity of the auxin transport system is determined by the PM abundance of PIN proteins, which was shown to be regulated by their sorting to and turnover in the lytic vacuole (Abas et al., 2006; Kleine-Vehn et al., 2008; Petrásek et al., 2006). In Chapter 3 of this thesis we showed that PIN phosphorylation by AGC3 protein kinases increases PIN PM abundance through a decrease in vacuolar PIN targeting. In fact, three of the AGC3 kinases, WAG1, WAG2 and AGC3-4 also showed nuclear localization and were able to decrease vacuolar targeting of PIN1 in a PIN phosphorylation-independent manner (Chapter 3). Although the mode of action for these kinases in the nucleus remained

unknown, previous research showed that dark-incubation of seedlings causes rapid turnover of PIN1 and PIN2 in the root by enhanced vacuolar targeting (Baster et al., 2012; Leitner et al., 2012; Marhavý et al., 2011). Furthermore, in weak *cop1* and *cop9/csn8* mutants this vacuolar targeting is equal in light or dark, whereas *hy5* mutants show enhanced PIN turnover even in the light, suggesting that COP1 and HY5 also function in the turnover of PIN1 and PIN2 (Laxmi et al., 2008; Sassi et al., 2012). *hy5* loss-of-function mutants have an increased number of lateral roots and a shorter main root and HY5 acts on many auxin related genes, promoting growth (Cluis et al., 2004; Sibout et al., 2006). Recently HY5 has been shown to act as a mobile signal from shoot to root to modify root growth by acting on nitrogen uptake (Chen et al., 2016). These observations raise the possibility that the AGC3 kinases and COP1/CSN function in overlapping pathways to stimulate or modify root growth, via PIN trafficking and auxin transport.

Here we investigated a putative nuclear function of the AGC3 kinases, and found that the predominantly PM localized PID can reduce PIN1 vacuolar targeting independent of PIN phosphorylation, when this kinase is targeted to the nucleus. Moreover, PID and AGC3-4 were found to interact with COP9/CSN8 and COP1, and to phosphorylate COP1 and another CSN subunit CSN7 *in vitro*. Dark germinated seedlings overexpressing *PID* (*35S::PID*) showed early loss of the apical hook, but when a nuclear targeted PID (*35S::SV40PID*) or AGC3-4 (*35S::AGC3-4*) were overexpressed, clear constitutive photomorphogenesis phenotypes could be observed in dark grown seedlings. Together this presents evidence for a new link between auxin transport and the regulation of photomorphogenesis by COP1.

Results

Nuclear localized PID and AGC3-4 stabilize PIN PM abundance independent of PIN phosphorylation

In Chapter 3 we showed that PID phosphorylation at conserved TPRXS sites in PIN1 and PIN2 is able to inhibit PIN1 and PIN2 vacuolar targeting. The AGC3 kinases WAG1, WAG2 and AGC3-4 were able to inhibit vacuolar targeting of PIN1-GFP S1,2,3A, a feat that PID was not able to perform. A key difference between PID and the other three kinases was that PID predominantly localized to the PM, whereas the other three kinases also localized to the nucleus, suggesting that the PIN phosphorylation-independent effect on PIN PM abundance was related to the activity of WAG1, WAG2 and AGC3-4 in the nucleus. In order to investigate this option, we generated a construct encoding a fusion protein between the SV40 nuclear localization signal and PID. Whereas wild-type PID was able to only inhibit vacuolar sorting of the wild type PIN1-GFP version, SV40-PID was able to inhibit

vacuolar targeting of both the wild-type PIN1-GFP and the phosphomutant PIN1-GFP S1,2,3A version, in a similar manner as the nuclear localized AGC3-4 kinases (Fig 1A). To investigate the effects of nuclear localized PID we generated *Arabidopsis* lines transgenic for the *35S::SV40-PID-RFP* overexpression construct. The localization in of SV40-PID in these lines and in protoplasts was indeed nuclear, but at the same time we observed PM localization (Fig. 1B-D). This result showed that the PIN phosphorylation-independent effect of the AGC3 kinases is related to their nuclear localization, which made us wonder which nuclear kinase targets would be mediating this effect on PIN trafficking.

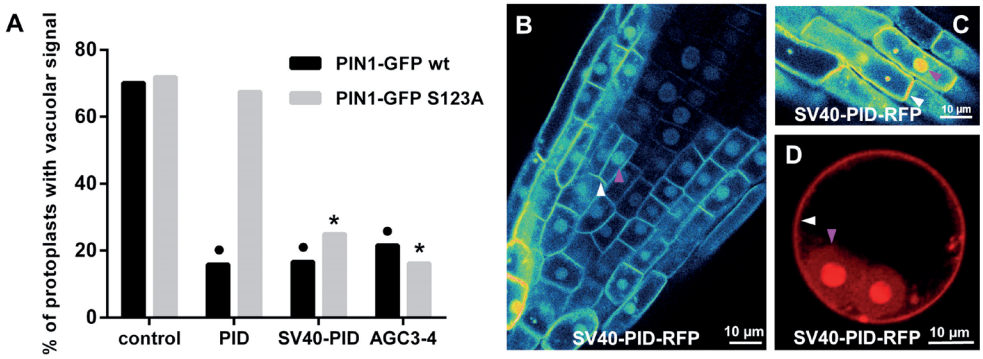

Figure 1: Nuclear SV40-PID and AGC3-4 reduce PIN1 vacuolar targeting in a PID-phosphorylation independent manner.

(A) *Arabidopsis* cell suspension-derived protoplasts were transfected with *35S::PIN1-GFP* or *35SS::PIN1-GFP S1,2,3A* (Huang et al., 2010) alone (control) or in the presence of *35S::PID-YFP* (PID), *35S::SV40-PID-YFP*, or *35S::AGC3-4* (AGC3-4). The transfected protoplasts were incubated in darkness for 20 hours and the number of cells with vacuolar PIN1-GFP were counted (at least 40/treatment). Black dot indicates significant difference with PIN1-GFP wt control (χ^2-test, $p<0.05$). Asterisk indicates significant difference with PIN1-GFP S123A control (X2-test, $p<0.05$). (B-D) Confocal microscopy images of *35S::SV40-PID-RFP* plants (B and C) and protoplasts transfected with *35S::SV40-PID-RFP* (D). Pink arrowhead indicates nuclear signal, white arrowhead indicates plasma membrane localization.

(SV40-)PID and *AGC3-4* overexpression lead to constant photomorphogenesis phenotypes.

We compared the seedling phenotypes of weak and strong *35S::SV40-PID-RFP* overexpression lines with those of *35S::PID-21* (strong overexpression line), *35S::PID-RFP* (weak overexpression line) and *35S::AGC3-4-YFP* plants (weak and strong line) (see also Chapter 2) and noticed effects on etiolated growth, so we chose to investigate this further and compared the weak and strong lines of *PID* (*35S::PID*), *AGC3-4* (*35S::AGC3-4*) and *SV40-PID* (*35S::SV40-PID*) (Fig. 2A-G). After five days of dark growth the *35S::PID* and *35S::AGC3-4-YFP* seedlings had shorter main roots and shorter hypocotyls than Col-0. Roots of *35S::SV40-PID-RFP* were longer and hypocotyls were shorter as well (Fig. 2J,K). The shorter main root length of *35S::PID-21* was probably caused by main root meristem

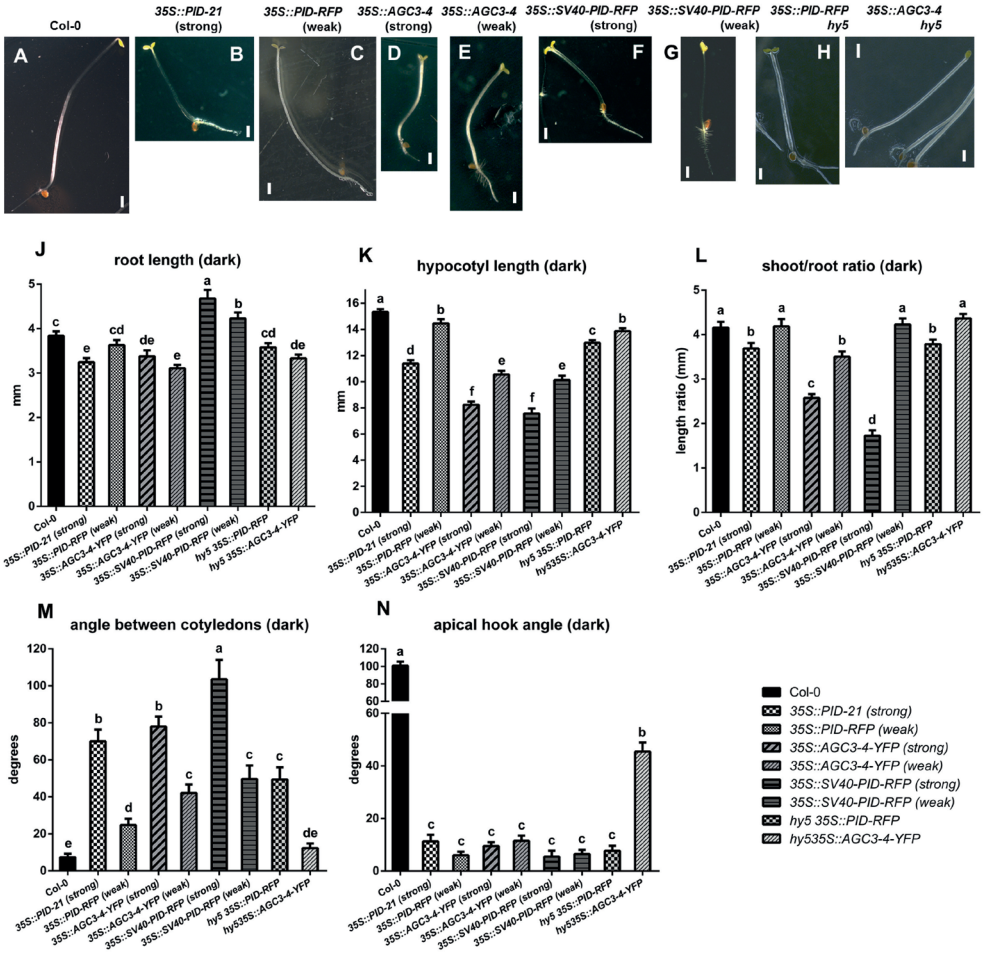

Figure 2: *35S::PID* decreases root growth, while *35S::SV40-PID* increases it and both have impaired apical hook maintenance and shorter hypocotyls.

(A-I) Representative pictures of five day old etiolated seedlings analyzed in (J-N) (scale bars are 1 mm). (J-N) Quantifications of etiolated growth phenotypes of lines depicted in (A-I) at five days of growth. (J) Main root length, (K) hypocotyl length, (L) Ratio between shoot and root (hypocotyl length/root length). (M) Angle between cotyledons. (G) Apical hook angle with hypocotyl. Letters denote different significant classes after One-way ANOVA and post-hoc Fischer test ($p<0,05$).

collapse (Fig. 2B) (see also: Benjamins et al., 2001), of which *35S::SV40-PID-RFP* had a lower rate. Hypocotyls of *35S::SV40-PID-RFP* were significantly shorter than those of *35S::PID* and at the same level as *35S::AGC3-4*. When comparing the shoot/root ratios the strong *35S::SV40-PID* line was significantly the lowest (Fig. 2L). Next we analyzed cotyledon opening and apical hook maintenance and noticed large differences between Col-0 and all the overexpression lines (Fig. 2M, N). These shorter hypocotyls, opened cotyledons and longer main root length are phenotypes reminiscent of weak constitutive photomorphogenesis mutants, such as *cop1-4*

(Deng et al., 1992). *35S::SV40-PID* lines had the strongest photomorphogenic phenotype, followed by *35S::AGC3-4* and *35S::PID*, with the stronger overexpression lines having the strongest phenotype. Especially the shoot/root ratio of strong *35S:SV40-PID* lines was striking and getting close to growth in low light levels. Since these results gave indications that (SV40)PID and AGC3-4 were involved in photomorphogenesis we crossed a *hy5* mutant, HY5 being the target of COP1 and a positive regulator of photomorphogenesis, through the weak *35S::PID-RFP* and *35S::AGC3-4-YFP* lines and noticed that this partially rescued the photomorphogenic phenotypes (Fig. 2J-N). The effect on *35S::PID* was not as strong, however *hy5* restored the cotyledon angle of *35S::AGC3-4* to Col-0 levels, while apical hook opening was restored half that of Col-0 (Fig. 2M,N). Adult *35S::PID* plants developed fairly normal except for a slight decrease in size, whereas *35S::AGC3-4 and 35S::SV40-PID* and plants were progressively smaller (Fig. 3A-D). Conversely to the partial rescue effect in seedlings, *hy5 35S::PID* and *hy5 35S::AGC3-4* plants were even smaller than the same overexpression lines in wild type background. (Fig. 3E-G). The same effect was observed in the *hyh 35S::PID* mutant (Fig 3H), while the *hy5 hyh* double mutant had a similar size to wild type (Fig 3I).

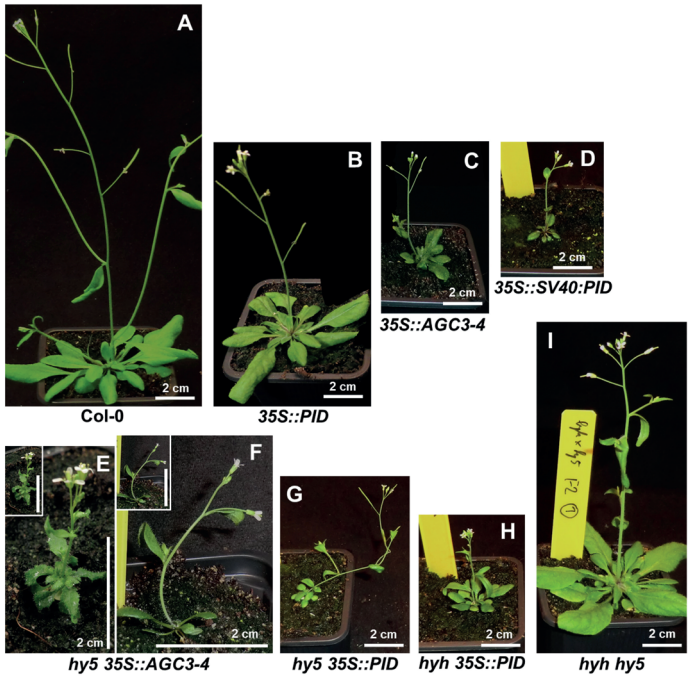

Figure 3: *35S::SV40-PID* resembles *35S::AGC3-4* in adult and etiolated seedling growth, while *hy5* and *hyh* increase *35S::AGC3-4* and *35S::PID* phenotypes.

(A-G) Representative pictures of overexpression lines after 5 to 6 weeks of growth in long day. (A) Wild type *Col-0*, (B) *35S::PID,* (C) *35S::AGC3-4* and (D) *35S::SV40-PID* overexpression. (E and F) *hy5 35S::AGC3-4* (Inset shows true size relative to other plants.), (G) *hy5 35S::PID* and (H) *hyh 35S::PID* displayed stronger dwarfism then the overexpression lines in Col-0 background. (I) A *hyh hy5* double mutant did not display dwarfism similar to the overexpression lines.

These results show that AGC3-4, PID and especially nuclear SV40-PID are involved in regulating photomorphogenesis, especially since *hy5* rescued the cotyledon opening defect of *35S::AGC3-4* in the dark. However, *hy5* increased the adult phenotypes of *35S::PID* and *35S::AGC3-4,* which does not fit with the seedling data and indicates that they PID and AGC3-4 probably not act directly on HY5.

PID and AGC3-4 interact with CSN8 *in vivo*

In a previous yeast two hybrid screen (Benjamins et al., 2003) we identified CSN subunit 8 (CSN8/COP9) as an interactor of PID (Fig. S1A). This interaction was confirmed using an *in vitro* protein pull-down assay (Fig. 4A and S1B), and subsequently *in vivo* using bi-molecular fluorescence complementation (BiFC) in *Nicotiana tabacum* leaf epidermis cells (Fig. 4B). An *in vitro* pull down assay with different PID deletion mutants showed that CSN8 interacts with the N-terminal part of PID. Expression of a CSN8-YFP fusion in protoplasts showed that the protein localized both to the cytoplasm and the nucleus (Fig. S1C), but in the BiFC experiment no interaction between PID and CSN8 could be observed in the nucleus. Still, in *Arabidopsis* protoplasts we were able to see strong sequestration of PID to the cytoplasm, and mild translocation to the nucleus when CSN8 was co-expressed (Fig. S1C). This nuclear sequestration was more pronounced in protoplasts that were incubated in the dark (Fig. S1C), which is interesting from the viewpoint that CSN8 is involved in dark/light signaling. Of the other three AGC3 kinases, AGC3-4 also was able to pull down CSN8 (Fig. 4C), although it was not clear with which domain. Interaction between AGC3-4 and CSN8 was confirmed in a BiFC assay and while PID interacted only in the cytoplasm, AGC3-4 interacted both in the nucleus and cytoplasm (Fig. 4C,D). However, we could not detect a BiFC signal when YN-WAG1 or YN-WAG2 were coexpressed in protoplasts with YC-CSN8 (not shown). Since CSN is an essential component of 26S proteasome-mediated protein degradation machinery involved in re-activation of E3 Ubiquitin ligases (Nezames and Deng, 2012), we investigated if PID itself is a target for proteasome-mediated degradation by treating *pid PID::PID-(venus)YFP* plants with the 26S proteasome inhibitor MG132. This treatment resulted in a marked increase in PID-YFP signal in the root meristem and the elongation zone, where PID-YFP was previously not visible (Fig. S1D-G). Interestingly, whereas we were unable to detect a nuclear localization of PID in untreated PID-CFP expressing protoplasts or tissues of *pid PID::PID-YFP* plants, we observed nuclear PID-YFP after MG132 treatment. This hinted at the possibility that PID is degraded in the nucleus. PID ubiquitination has been shown to happen in biochemical experiments (Maraschin, thesis, Chapter 5, Fig. 6). In contrast, AGC3-4-YFP did not respond to MG132 treatment (data not shown). Overall, the interaction of AGC3-4 and PID with CSN8 and their partial nuclear localization indicated that these AGC3 kinases, known for their PM-associated activity may also function in the nucleus and that most likely (at least for PID) their activity is regulated by proteasome-mediated degradation in the nucleus.

Assessing the role of PID as a putative regulator of the CSN

Several kinases have been shown to interact with the CSN, and in this way they can regulate the turnover of proteins that targets for proteasome degradation by phosphorylating these targets (Uhle et al., 2003), or regulate the activity of the CSN itself by phosphorylation of CSN subunits (Bech-Otschir et al., 2001). *In vitro* phosphorylation assays showed that PID did not phosphorylate CSN8 (Fig. S2A). However, when we tested the CSN subunit 7 (CSN7/COP15/FUS5), which is a known phosphoprotein (Karniol et al., 1999) and associates with CSN8 in the CSN (Serino et al., 2003), we observed a low but significant phosphorylation signal (Fig. S2A). Using the NetPhos software and by incubating synthetic peptides representing the predicted phospho-sites with PID in *in vitro* phosphorylation reactions, two putative phosphorylation sites (S19 and T20) were identified in CSN7 (Fig. S2B,C). The sequence context of S19 (KRxST) matched the conserved PRXS PID target sequence present in PIN proteins. Mutating either S19, T20, or both residues to Alanine abolished phosphorylation of CSN7 by PID in an *in vitro* phosphorylation assay (Fig. S2D). However, when the wild-type protein or these mutants were analyzed for complementation of the *cop15-1* mutant allele (Table 1). The reduced number of seedlings showing the mutant phenotype (8% instead of 25%) has been were subjected to *Arabidopsis* seedling extracts, all protein versions were phosphorylated at the same level (Fig. S2E). Moreover, an *in vitro* phosphorylation assay where CSN7 was exposed to protein extracts from different *PID* mutant seedlings showed no significant difference in phosphorylation of CSN7 (Fig. S2F). These results indicated that S19 and T20 are probably not the predominant phosphorylation sites in CSN7, and also that PID is most like not efficiently phosphorylating CSN7 *in vivo*. In order to check the function of S19 and T20 *in vivo*, we generated Arabidopsis lines transgenic for the *CSN7::CSN7-mRFP* construct, or for mutant versions encoding fusion proteins with either the S19 to A, T20 to A or the S19 and T20 to DD substitutions (DD was used to mimic phosphorylation). The resulting homozygous transgenics were crossed with the *cop15-1* allele and the F2 plants reported before for this allele, and is explained by the frequent embryo lethality among the homozygous progeny (Dessau et al., 2008). All constructs were able to significantly reduce the number of seedlings showing *cop* mutant phenotypes, and for all constructs phenotypically wild type transgenic plants could be obtained that were homozygous for *cop15-1* and showed strong CSN7-mRFP expression in meristematic and vascular tissues (Fig. S3). These results show that all constructs are able to complement the *cop15-1* mutant, corroborating our previous conclusion that S19 and T20 are not functional phosphorylation sites in CSN7, and that phosphorylation of CSN7 by PID is not important for normal seedling development. However, more subtle assays where plants are grown under less optimal conditions might yield different results for these particular mutants. Based on these results we concluded that the association of PID and AGC3-4 with the CSN is not to regulate CSN activity, but rather to regulate the activity of other CSN-interacting proteins.

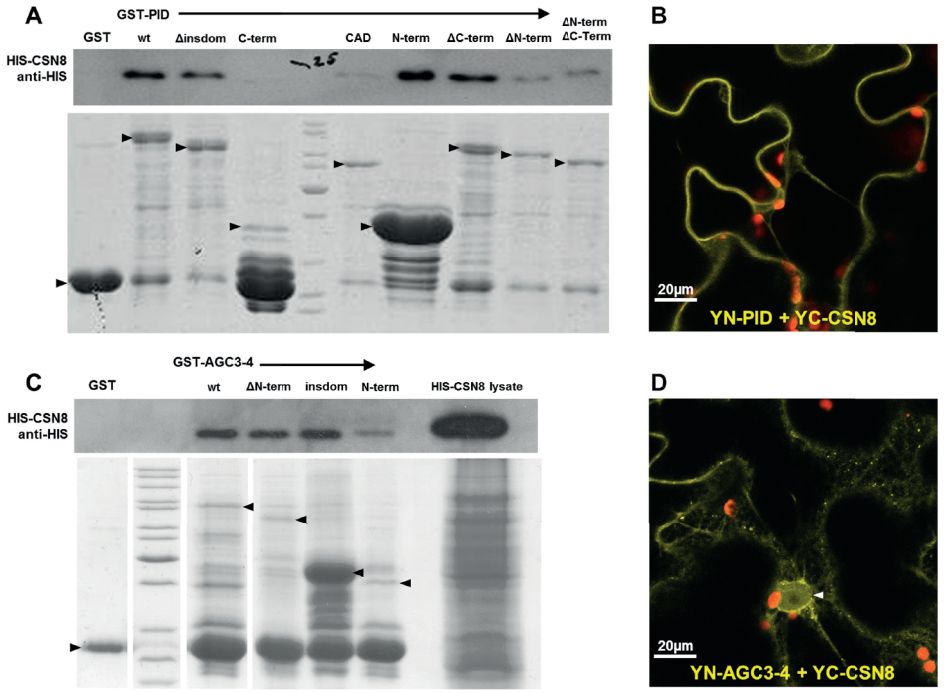

Figure 4: PID and AGC3-4 interact with CSN8 in the cytoplasm and nucleus.
(A) *In vitro* pull-down of HIS-tagged CSN8 by GST-tagged PID and mutant versions thereof: Δinsdom = AGC3 insertion domain deleted, CAD = kinase domain without N- and C-terminal domains, ΔN-/C-term = deleted N-/C-terminal and ΔNtermΔCterm = both domains deleted, (for domain details, see methods)). A GST-only reaction and HIS-CSN8 lysate were loaded on the SDS-PAGE. As a loading control a coomassie stained gel is shown with the same experiment loaded. (B) BiFC experiment performed by *Agrobacterium* transient transformation in *N. tabacum* leaf epidermis. Red signal is the autofluorescence of the chloroplasts and in yellow the cytoplasmic BiFC signal is visible between the N-terminal half of YFP (YN) N-terminally fused to PID and the C-terminal half of YFP (YC) N-terminally fused to CSN8. (C) *In vitro* pull-down of HIS-tagged CSN8 by GST-tagged AGC3-4 and mutant versions thereof (insdom = AGC3 insertion domain only). As a control a GST-only reaction and HIS-CSN8 lysate was loaded on the SDS-PAGE. A GST-only reaction and HIS-CSN8 lysate were loaded on the SDS-PAGE (Lanes were not in same order as western blot, see Fig. S6 for original image). (D) BiFC Cytoplasmic and nuclear (white arrowhead) BiFC signal between YN N-terminally fused to AGC3-4 and YC N-terminally fused to CSN8.

Table 1: PID phosphorylation of CSN7 does not have an obvious role in plant development.
Analysis of complementation of a *cop15-1* allele by a wild type CSN7, two phosphosite mutants (SA and AT) and a double phosphosite mimic mutant (DD). Per construct two different lines were tested and the resulting *cop* phenotypes counted. The ratio of wild-type to *cop* seedlings was compared to the segregating *COP15/cop15-1* background using the χ2 test.

Plant line	seedling #	non-cop	*cop*	% *cop*	p (χ2 test)
Cop15-1/cop15-1	**493**	**452**	**41**	**8.32%**	
CSN::CSN7 WT #6	**486**	**485**	**1**	**0.21%**	**<0.001**
CSN::CSN7 WT #8	**559**	**553**	**6**	**1.07%**	**<0.001**
CSN::CSN7 AT #1	**521**	**505**	**16**	**3.07%**	**<0.001**
CSN::CSN7 SA #7	**500**	**500**	**0**	**0.00%**	**<0.001**
CSN::CSN7 SA #8	**499**	**480**	**19**	**3.81%**	**<0.001**
CSN::CSN7 DD#1	**492**	**472**	**20**	**4.07%**	**<0.001**
CSN::CSN7 DD#2	**564**	**472**	**3**	**0.53%**	**<0.001**

PID and AGC3-4 interact with and phosphorylate COP1 in the nucleus

The clear constitutive photomorphogenesis phenotypes of *35S::(SV40-)PID* and *35S::AGC3-4* seedlings combined with the conclusion that PID and AGC3-4 might regulate other CSN binding proteins, prompted us to test for functional interactions with other components of the photomorphogenesis pathway. The CSN is known to regulate the activity of CULLIN ubiquitin ligase complexes and its key target in the photomorphogenesis pathway is the CUL4–DDB1$^{COP1-SPA1}$ E3-ligase (Nezames and Deng, 2012). The interaction with CSN8 sequestered PID towards the nucleus and AGC3-4 clearly interacted with CSN8 in the nucleus (Fig. 4D and Fig. S1C). A possible role for the interaction of PID and AGC3-4 with CSN8 could therefore be to bring the kinases in close proximity to the well-known photomorphogenesis regulator COP1. Studies in mammalian systems have shown that AGC kinases interact with the CSN to regulate the turnover of the COP1 targets p53 and c-jun by phosphorylation (Uhle et al., 2003). Transfection of *35S::PID-CFP* and *35S::AGC3-4-CFP* constructs in *N. tabacum* leaf epidermis cells using *Agrobacterium* infiltration showed that PID-CFP localized in the cytoplasm and at the plasma membrane and AGC3-4 in the cytoplasm and the nucleus (Fig. S4A,B). AGC3-4-CFP was visible in nuclear speckles (Fig. S4B), a result we also observed in stably transformed *35S::AGC3-4-YFP Arabidopsis* lines (Chapter 2). Transient expression of YFP-COP1 in tobacco epidermis cells also resulted in strong accumulation of the YFP signal in nuclear speckles (Fig. S4C). These structure are usually called photobodies when they contain active phytochromes, and are thought to contain a wide range of light signaling components such as the CSN, COP1, targets of COP1, and Phytochrome Interacting Factors (PIFs) (Van Buskirk et al., 2012). Transient co-expression of PID-CFP or AGC3-4-CFP and YFP-COP1 showed clear sequestration of PID to the nucleus, but no colocalization in nuclear speckles (Fig. 5A,B). In contrast, nuclear AGC3-4-CFP showed strong colocalization with YFP-COP1 in nuclear speckles (Fig. 5C,D). These results suggested that COP1 can interact with the PID and AGC3-4 kinases, and this was confirmed by *in vitro* pull-down assays (Fig. 5E,F).

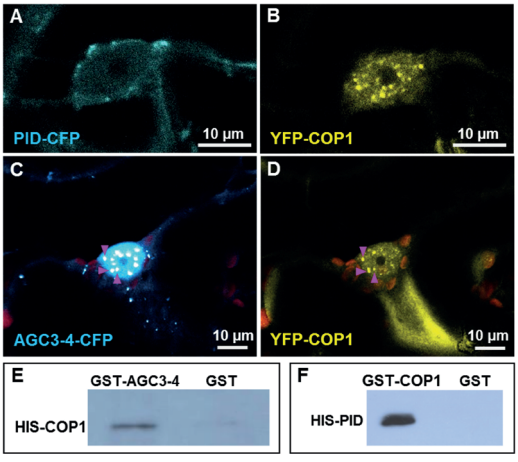

Figure 5: PID and AGC3-4 colocalize with COP1 in the nucleus and interact *in vitro*.
(A-D) Confocal microscopy images of *N. tabacum* leaf epidermis cells, co-transfected with *35S::PID-CFP* (A) and *35S::YFP-COP1* (B), or with *35S::AGC3-4-CFP* (C) and *35S::YFP-COP1* (D). In each picture the nucleus of a leaf epidermis pavement cell is visible and pink arrowheads indicate co-expression of AGC3-4-CFP and YFP-COP1 in nuclear speckles. (E) *In vitro* pull-down of HIS-COP1 by GST-tagged AGC3-4 or GST (F) *In vitro* pull-down of HIS-PID by GST-tagged COP1 or GST.

Next, we investigated the possibility that these kinases phosphorylate COP1. In an *in vitro* phosphorylation assay we observed a single phosphorylated band of the same molecular weight as COP1 when either AGC3-4 or PID were added to the reaction, and this band was not visible in a COP1-only control sample (Fig. 6A,B, lanes 1,2,8). Both kinases also phosphorylated the PIN2 hydrophilic loop (PIN2HL) in the positive control samples (Fig. 6A,B, lanes 5,6). A search for possible phosphorylated amino acid residues in COP1 detected serine 20 in the PRTS motif, which is strikingly similar to the AGC3 TPRXS motif phosphorylated in PINs (Huang et al., 2010). Substitution of serine 20 in COP1 to alanine resulted in the loss of AGC3-4 and PID mediated COP1 phosphorylation (Fig. 6A, lanes 3,4), showing that at least *in vitro* PID and AGC3-4 phosphorylated COP1 at a single residue . This also explained partially why the intensity of phosphorylated COP1 band was weaker than the band representing PIN2HL, which is phosphorylated by AGC3-4 and PID at three different residues (Dhonukshe et al., 2010) (Chapter 2). In analogy with animal systems, another possibility was that AGC3-4 and PID interact with COP1 in order to phosphorylate its downstream targets. However, one of the key COP1 targets HY5 was found not to be phosphorylated *in vitro* by either kinase (Fig. 6B, lanes 3,4), suggesting that the kinases act to regulate COP1 itself. An analysis of COP1 amino acid sequences from varying plant species showed that this PRTS motif in COP1 is conserved in plant species, however only weak or no conservation was found in evolutionary more distant species, such as the Solanaceae or monocots (Fig. 6C).

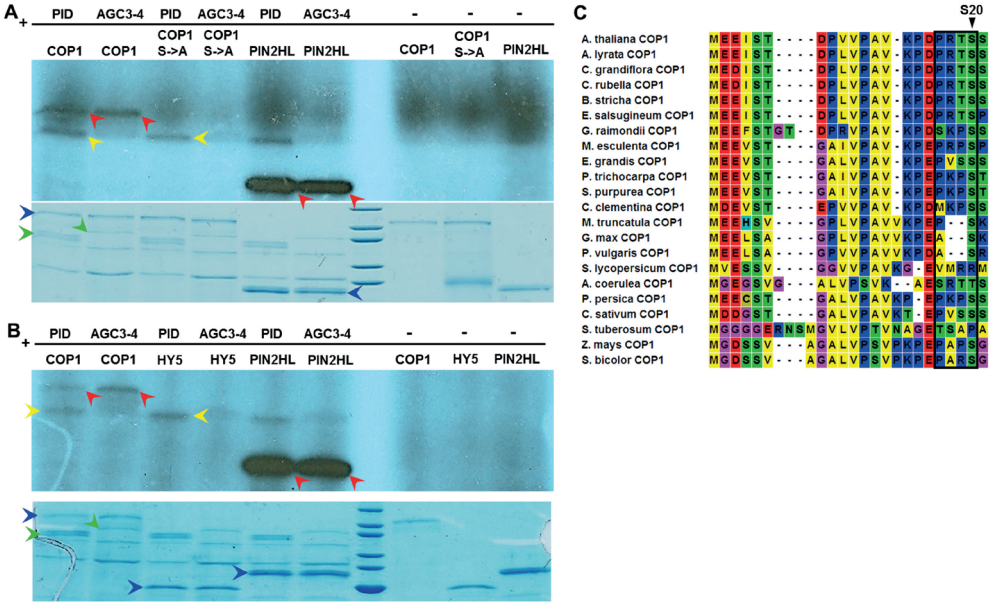

Figure 6: PID and AGC3-4 phosphorylate COP1 *in vitro* at a conserved N-terminal PRXS motif.
(A) Autoradiograph (upper panel) and corresponding Coomassie stained gel (lower panel) of an *in-vitro* phosphorylation assay of either PID or AGC3-4 kinase against GST tagged targets (blue arrow(: COP1, COP1

S20A (COP1 S->A) or the PIN2 hydrophilic loop (PIN2HL). PID is visible as a double band (green arrow), the upper of which corresponds to trans-auto-phosphorylated PID (yellow arrow). Red arrows show phosphorylation of targets. (B) Autoradiograph (upper panel) with corresponding Coomassie stained gel (lower panel) of an *in-vitro* phosphorylation assay of GST tagged PID and AGC3-4 kinases with GST tagged COP1, HY5 and PIN2HL as targets (blue arrows) and (green arrows). Red arrows show phosphorylation of targets. (C) An alignment of the N-terminal domains of several COP1 proteins from flowering plants. Serine 20 forms part of a conserved PRXS motif (black box) resembling the TPRXS motif found in PIN hydrophilic loops (Huang et al., 2010).

Discussion

A nuclear function for the AGC3 kinases seems an unlikely prospect at first, since their canonical targets, the PIN proteins are localized at the plasma membrane (Habets and Offringa, 2014). However, the results presented here provide strong indications that the AGC3 kinases PID and AGC3-4 do have a function in the nucleus and phosphorylate nuclear proteins, a fact that has been shown before in maize, where PID ortholog BARREN INFLORESCENCE2 is able to interact with and to phosphorylate the transcription factor BARREN STALK1 (Skirpan et al., 2008). In the case of Arabidopsis PID and AGC3- we found that the kinases interact with and phosphorylate two central components of the photomorphogenesis pathway, COP1 and the CSN and not transcription factor HY5. Etiolated growth of *35S::AGC3-4* and *35S::(SV40-)PID* lines showed that these kinases affect photomorphogenesis in a positive manner. The fact that the nuclear *35S::SV40-PID* lines had stronger photomorphogenic phenotypes than the non-nuclear *35S::PID* indicates that the nuclear function is associated with the effect on photomorphogenesis.

Crossing the *35S::AGC3-4 and 35S::PID* lines through *hy5* reduced the photomorphogenesis phenotype and again this happened more strongly in *35S::AGC3-4*. it is conceivable that phosphorylation of the CSN or COP1 by these kinases leads to inhibition of COP1 and a subsequent positive effect on HY5 protein levels, something that still needs to be shown. Exactly how this would happen molecularly remains unclear, although an obvious mechanism could be that Serine 20 phosphorylation might inhibit SPA binding to COP1. For example, UV-B radiation triggers the binding of UVR8 to COP1, which dissociates the SPAs, leading to decreased COP1 activity and increased HY5 (Hayes et al., 2014; Yin et al., 2015). Light-activated PHYA and PHYB also interact with the SPAs, leading again to COP1 inactivity and COP1 target accumulation (Sheerin et al., 2015).

A possible function for this proposed AGC3-kinases inhibition of COP1 might be found in the control of PIN vacuolar targeting (see also Chapter 2). In the *cop9-1* mutant background PIN2-GFP is resistant to dark-induced vacuolar targeting (Laxmi et al., 2008) and it has been shown that PIN1 and PIN2 vacuolar targeting in roots is under the control of COP1 (Sassi et al., 2012). Our results now showed that both AGC3-4 and nuclear localized PID can reduce PIN1 turnover independent of PIN phosphorylation. Therefore it is conceivable that PID and AGC3-4 modulate COP1 or the acquisition of downstream targets and thereby affect

PIN turnover. Furthermore, *35S::SV40-PID* promoted root growth in the dark, compared to Col-0, which is an important distinction since the main root increase in the dark is also seen in *cop1-4* and *cop1-6* (Sassi et al., 2012). In addition, SV40-PID inhibited darkness-induced vacuolar targeting, while weak cop1 lines were insensitive to this process.

An alternative (non-exclusive) possibility is that the interactions with CSN and COP1 are necessary for the degradation of PID and AGC3-4. In the case of PID that may be likely, since it is not localized in the nucleus under normal conditions (Dhonukshe et al., 2010) and application of MG132 increased PID signal and resulted in nuclear PID in certain tissues. AGC3-4 however is localized in the nucleus both in light and darkness (Fig. S5, Chapter 2). Degradation of PID by COP1 might occur at the same time that phosphorylation takes place and thus explain why PID can be sequestered to the nucleus, but is normally not strongly visible there. It would then follow that AGC3-4 is not degraded via this mechanism.

In Chapter 2 we showed that *35S::AGC3-4* plants showed a decreased flowering time relatively to wild-type plants under long day conditions. It is possible that this effect is due to the interactions with COP1, since it is known that COP1 mediates the day length signaling by ubiquitinating the flowering time regulator CONSTANS (Jang et al., 2008). The *cop1-4* mutant flowers early and has a very similar phenotype to *35S::AGC3-4* and *35S::SV40-PID*, which is in line with the proposed role of PID and AGC3-4 as negative regulators of the COP1 pathway that represses photomorphogenesis and flowering. It would be interesting to look for defects in other known COP1 associated processes, such as shade avoidance (Crocco et al., 2010; McNellis et al., 1994), or UV-B-mediated DNA damage control (Hayes et al., 2014).

It is important to note that any phenotypes attributed to *35S::SV40-PID* are of course artificial. In normal conditions we did not observe *PID-YFP* in the nucleus, however this did happen when the 26S proteasome was inhibited. PID nuclear localization may be a very transient event, whereby it carries out its function and then is quickly degraded. However, since AGC3-4 is often observed in the nucleus, it is likely that it is mainly AGC3-4 which carries out the nuclear function of the AGC3 kinases.

Regulation of COP1 and the CSN by PID and AGC3-4 might form an additional feedback loop between light signaling and PIN-driven polar auxin transport. Known mechanisms where light affects the polarity of polar auxin transport by repressing PID-dependent PIN phosphorylation are for example, enhanced hypocotyl elongation by far-red light enrichment (Keuskamp et al., 2010), inhibition of dark induced PIN vacuolar targeting in the root, upon light stimulation of the shoot (Sassi et al., 2012) and hypocotyl and root bending by unidirectional blue light (Ding et al., 2011; Preuten et al., 2013; Zhang et al., 2013). In all these examples, light reduces *PID* transcription, which subsequently leads to changes in the PIN polar distribution. Because of the light signaling-mediated reduction in *PID* expression, it is unlikely that PID itself plays a role in repressing COP1

activity in aboveground tissues. This role is likely to be mediated by AGC3-4, for which we showed here that its expression is enhanced in the light. A possible role for PID could be to enhance PIN PM abundance in the dark grown root system, by repressing COP1 and CSN function when the shoot is grown in the light. The signal that triggers PID activity in the roots could be auxin transported from the shoot to the root, since *PID* is induced by auxin itself. PID (and possibly AGC3-4) could relay that auxin signal towards PIN stability, both directly by phosphorylation of the TPRXS motifs and indirectly by negative regulation of COP1, strengthening the effect. Alternatively, HY5 can act as a mobile shoot to root signal (Chen et al., 2016) and bind the promoter of PID (Lee et al., 2007), however it is not clear if this would lead to suppression or enhancement of *PID* expression. The role of COP1 could be the direct ubiquitination of PINs, which would lead to vacuolar targeting (Leitner et al., 2012), or COP1 could affect PIN vacuolar targeting through degradation of its targets, which opens up a myriad of possibilities, since HY5 and HYH have opposing functions in root growth, but are both degraded by COP1 (Sibout et al., 2006). By regulating COP1 the AGC3 kinases PID and AGC3-4 could thus promote root growth in the dark, although further investigation into the precise molecular mechanisms and biological relevance is needed to shed more light on this matter.

Materials and methods

Plant material and growth conditions

Nicotiana tabacum leaves of two to four week old plants were used for agroinfiltration in a Bi-molecular Fluorescence Complementation (BiFC) and colocalization assays. *Arabidopsis* mutant alleles *cop1*-SALK137391, *cop1*-SALK027212, *hy5*-SALK056405, *hyh*-WiscDsLox253D10 are in Col-0 background and *cop15-1 (csn7)* in *Ler* background. The *pid-14 PID::PID-YFP, agc3-4 AGC3-4-YFP* and *35S::AGC3-4-CFP/YFP* lines are described in Chapter 3. Arabidopsis genotypes used for the CSN8/CSN7 *in vitro* phosphorylation assay of Fig. S2 were wild-type Col-0, *pid-14* (SALK_049736), *pid-14 wag1 wag2* loss-of-function mutants (Dhonukshe et al., 2010), the 35S::PID-21 (Benjamins et al., 2001) and the tamoxifen-inducible pINTAM>>PID (Friml et al., 2004) overexpression lines. *hy5 35S::PID-RFP, hy5 35S::AGC3-4-YFP* and *hyh 35S::PID-RFP* lines were obtained by crossing a *35S::PID-RFP* (line 174, from (Dhonukshe et al., 2010)) or *35S::AGC3-4-YFP* (T3#12-1) with the *hy5* or *hyh* allele. All primers for genotyping can be found in table S1. For plate growth, *Arabidopsis* seeds were surface sterilized by a 30 seconds wash with 70% ethanol, followed by 10 minutes incubation in 50% commercial bleach solution (1% chlorine). Seeds were subsequently rinsed five times with sterile water. Seeds were vernalized for 5 days in dark at 4°C and germinated on ½ MS medium supplemented with 1% sucrose and 0.8% Daichin agar and antibiotics when required (21°C, 16 h-photoperiod, 70% humidity and a PAR of 70-

90 µmol/m^2/s). For the experiments in Fig. 3 the sucrose was omitted from the ½ MS. At least 30 seedlings per genotype were analyzed to obtain the data in Fig. 3. For MG132 treatment, 5 day old seedlings were placed in liquid ½ MS with 1% sucrose containing 50 µM MG132 or DMSO for four hours, after which they were mounted in ½ MS on slides and imaged using confocal microscopy. For plant growth on soil, seeds were sown onto soil after overnight vernalization on wet filter paper in the dark at 4°C, or they were transferred to soil after two weeks of growth on agar plates. Plants were grown at 21°C and 70% relative humidity with a 16 hour photoperiod (PAR 140 µmol/m2/s).

Molecular cloning

All oligonucleotides used for cloning are listed in table S1. The pGEX-PID (Benjamins *et al.*, 2003) and pGEX-PIN2HL (Abas *et al.,* 2006) constructs have been described previously. The coding regions of *PID, AGC3-4*, *CSN7, CSN8* and *COP1* were amplified from *Arabidopsis thaliana* ecotype Columbia (Col-0) cDNA and the *HY5* coding region was obtained from a RAFL cDNA clone from the RIKEN institute (clone id: pda19772), using the Gateway cloning primers described in table S1 and cloned into pDONR207 using BP recombinase (Invitrogen). The *SV40-PID* fusion was obtained by amplifying the PID coding region from the pDONR clone using Gateway primers containing the SV40 tag. The fragment was subsequently BP recombined into pDONR207. PID and AGC3-4 domain mutants were constructed by gateway cloning from cDNA with specific attB primers (Table S1). PID ΔN-term = AA 75-438, PID ΔC-term = AA 1-401, PID ΔN-ΔC-term = AA 75-401, PID N-term = AA 2-103, PID C-term = AA 339-438 and PID CAD = AA 75-398. AGC3-4 N-term = AA 1-99, AGC3-4 insdom = AA 232-348, AGC3-4 ΔN-term = 100 – 525.

The mutant CSN7 constructs were made with pDONR207:CSN7 using the Quickchange XL site-directed mutagenesis kit (Stratagene) as described previously (Dhonukshe et al., 2010). The construction of *pART7*-based CFP/YFP/mRFP Gateway destination vectors was described previously (Dhonukshe *et al.*, 2010). For YFP-COP1 transient transfection assays a pUNI-COP1 cDNA clone (obtained from ABRC) was Cre/Lox recombined into pNIGEL19 (Geldner et al., 2009) to yield a UBQ::YFP-COP1 containing binary vector plasmid. To create COP1 SA/SE mutants, pDONR-COP1 was used for site directed mutagenesis through a protocol adapted from Sawano and Miyawaki, 2000: A 5′ phosphorylated primer containing the desired base-pair changes and also a novel restriction site were used in a ligation-Phusion based PCR to replicate the template plasmid with the desired base-pair change, followed by *Dpn*I digestion of the original template plasmid. This mix was transformed into DH5α and colonies were screened by colony-PCR and restriction enzyme digestion of the resulting PCR fragments for the newly introduced restriction site. For the CSN8 BiFC assay, the pUBC/pUBN YN/YC vectors (Grefen et al., 2010) were used and the CSN8/AGC3-4/PID constructs were Gateway LR-recombined into these destination vectors

using the pDONR207 entry vectors described above. Expression vectors pGEX-PID, pGEX-AGC3-4, pGEX-COP1(SA), pGEX-HY5, pART7-PID-CFP, pART7-PID-mRFP, pART7-WAG1-mRFP, pART7-WAG2-mRFP, pART7-AGC3-4-CFP/mRFP and pGREEN229-CSN7::CSN7(SA/AT/DD)-mRFP were constructed by LR recombinase-mediated cloning of the appropriate coding region into either the pGEX-based destination vector for N terminal fusions with the *Glutathione-S-transferase* (*GST*) coding region, or into the pART7-based destination plasmids for overexpression in *Arabidopsis* protoplasts. For stable transformation of the *35S::PID*, *35S::SV40-PID*, and *35S::AGC3-4* overexpression lines expression cassettes of pART7-AGC3-4-mRFP and pART7-(SV40)PID-mRFP were cloned into the pART27 binary vector (Gleave, 1992) by *Not*I digestion and ligation. DH5α strain *E. coli* were grown on LB medium supplemented with 100 µg/mL carbenicillin for pART7 or pGEX-based plasmids, 10 µg/mL gentamicin for pDONR207, 100 µg/mL spectinomycin for pUBC/pUBN vectors, or 25 µg/mL kanamycin for pNIGEL19 or pART27 vectors. *E. coli* DH5α was transformed by electroporation. Binary plasmids were introduced into *Agrobacterium tumefaciens* strain AGL1 (containing the pSOUP plasmid) by electroporation and selection on LC medium containing 20 µg/ml rifampicin and 75 µg/mL kanamycin (pART27 and pNIGEL19), or 100 µg/mL spectinomycin (pUBC/pUBN). For the CSN8 BiFC assay the pUBC/pUBN YN/YC vectors (Grefen et al., 2010) were used and the CSN8/AGC3-4/PID constructs were Gateway LR-recombined into these destination vectors using pDONR207 entry vectors.

Yeast two-hybrid

The Matchmaker yeast two-hybrid system (Clontech, Palo Alto, CA) was used to screen two Arabidopsis cDNA libraries fused to the GAL4- activation domain (pACT) with a PID:GAL4-DNA-binding domain (pAS2-1) fusion. One cDNA library was constructed using mRNA isolated from green parts of 6-week-old flowering Arabidopsis plants. The second cDNA library was constructed using a 1:1 ratio of mRNA from auxin-treated (1µM 1-naphthaleacetic acid for 24 h) and wild-type roots of 10-d-old Arabidopsis seedlings. The yeast strain PJ69-4a (James et al., 1996) containing pAS2-1-PID was transformed with each of the pACT cDNA libraries (Gietz et al., 1992), and was screened for His and adenine auxotrophy. Growth rates of transformants were compared with controls (the wild-type strain and the wild-type strain containing only pAS2-1-PID). When screening for adenine auxotrophy, reddening of the colonies was used as an indication for the strength of interaction. Screens were performed at 20°C and 30°C. α-Galactosidase assays in liquid yeast cultures were performed as described (Meijer et al., 2000).

Plant transformation

Arabidopsis 35S::AGC3-4-mRFP, 35S:PID-mRFP, and *35S::SV40-PID-mRFP* plant lines were obtained by *Agrobacterium*-mediated transformation of Col-0 by floral dipping (Davis et al., 2009) using *Agrobacterium* strain AGL1 containing the *pART27:35S::PID-RFP* or *pART27:35S::AGC3-4-RFP* plasmids. T1 and T2 generations were selected on plates with timentin (only T1, 100mg/l) and 25mg/l kanamycin. T2 plants were screened for single locus T-DNA inserts, and homozygous transgenic lines were selected in the T3 generation using antibiotic resistance. Using the same method, *cop15 CSN7::CSN7-mRFP(SA/AT/DD)* complementation lines were obtained by transforming the pGREEN229-CSN7::CSN7(SA/AT/DD) construct into heterozygous and *cop15/+* plants. Primary transformants were selected with 30mg/l ppt for the t-DNA inserts and 25mg/l kanamycin for the *cop1* allele, while T1 transformants of *cop15/+* were genotyped for the mutant allele. T2 and T3 plants were screened as described above.

Transient expression in tobacco leave cells by *Agrobacterium* infiltration.

Agrobacterium strain AGL1 containing the desired expression plasmid was grown in liquid culture until saturation. This starter culture was used to inoculate (1:100 -> 1:200) 60 ml of medium containing antibiotics and grown o/n to OD600 of 0.3->1.0. The culture was spun down at 4000 rpm for 30 minutes and the resulting pellet resuspended in MS medium with 2% sucrose and 1g/L MES (pH5.6), containing 20 µM acetosyringone. The suspension was left in the dark at RT for at least one hour to induce the *Agrobacterium* virulence genes, and subsequently used to infiltrate. the underside of *Nicotiana tabacum* leaves using 2ml syringes. Following infiltration, plants were covered with plastic bags for a few hours at normal growth conditions. After two days of incubation in normal growth conditions leaves were observed with confocal microscopy.

Protoplast isolation and transformation

Arabidopsis thaliana Col-0 cell suspension cultures were used for protoplast preparations. Culture maintenance, protoplast isolation and transfections were performed as previously described (Schirawski et al., 2000) with minor modifications. Four- to six day old cultures were diluted 5-fold in Cell Medium (30 g /L sucrose, 3.2 g/L Gamborg's B5 basal medium with mineral organics, adjusted to pH 5.8 with KOH and sterilized by autoclaving), incubated overnight and used for protoplast isolation. Following transfection with 10µg plasmid DNA per $1*10^6$ protoplasts, the cells were incubated at 25 ^oC in the dark for 16-18 hours before observation or additional treatments.

Confocal microscopy and analysis

For confocal images of roots, four- to seven day old seedlings were mounted in water or ½ MS on glass slides. Roots were imaged using an upright Zeiss LSM5 LCSM with a 458 (CFP)/ 488(GFP)/ 514(YFP)/ 543(mRFP)nm argon laser and 475-525 nm, 505-530 nm, 530-600 nm, or 560-615 band pass emission filters for CFP, GFP, YFP, or RFP, respectively and a CCD camera. For each excitation filter, the autofluorescence was captured by placing a long-pass 650nm filter in front of the detector. Root images were captured with a 40x 1.2NA water objective. Overnight-incubated protoplasts were pipetted into 8-well coverslips and imaged with an inverted Zeiss LSM5 microscope with an 63x 1.3NA oil objective using the same laser and band-pass filters as described above for the upright LSM5. *N. tabacum* leaves were imaged with a 40x 1.2NA water objective using the inverted Zeiss LSM5 microscope by mounting the tissues on a glass petri dish with thin bottom in water with a cover slip covering the leaf and held down by a small metal object. Images were quantified using ICY bioimage analysis software (http://icy.bioimageanalysis.org/download) and subsequently assembled into figures using GIMP (https://www.gimp.org/).

Pull-down and western blot

E. coli lysates containing the proteins of interest were produced by diluting 5ml of overnight culture in 50ml of fresh LC medium supplemented with antibiotics and growing this culture at 37 ˚C to an OD_{600} of 0.4-0.8. The cultures were subsequently induced for 4 hours with 0,4 mM of IPTG. After induction, the cultures were centrifuged at 4000 rpm for 20 min and the pellets were stored at -20˚C. Pellets were resuspended in fresh extraction buffer (1x PBS, 2 mM EDTA, 2 mM EGTA, 2mM DTT, 150 mM NaCl pH 8, supplemented with 1 mM PMSF with protease inhibitor tablets from Pierce (1 tablet/20ml buffer) and 1 mg/ml lysozyme) and incubated for 1 hour at 4˚C on a rocking table. Cells were sonicated (on ice) and cell debris was centrifuged at 14000rpm at 4˚C for 30 minutes. After addition of 1% triton, the supernatant (containing the expressed protein) was divided into 100µl aliquots. For pull-down, 100µl of GST-tagged lysate (in total 500 µl extraction buffer) was bound to glutathione agarose beads for 2 hours at RT. 100 µl of each HIS-tagged protein was added to the GST-tagged protein loaded beads and binding buffer (50 mM Tris pH 6, 200 mM NaCl, 0,1% Tween 20) was added to a total reaction volume of 400 µl. The samples were then incubated at RT for 2 hours on an Eppendorf rotator. After incubation, the resin was washed 3 times in 500 µl wash buffer (25 mM Tris-HCL pH 8, 10% glycerol, 300 mM NaCl, 20 mM imidazole, 0,05% Tween 20) with in-between centrifugation at 4000 rpm for 3 minutes. 40 µl of 1x SDS-PAGE loading buffer (40% glycerol, 240 mM Tris/HCl pH 6,8, 8% SDS, 0,04% bromophenol blue, 5% β-mercaptoethanol) was added to the precipitated resin and samples were boiled at 99˚C for 10 minutes. The boiled resin was spun down and the supernatant was transferred to a 12,5% polyacrylamide gel for SDS page. Blotting of

the proteins onto a PVDF membrane was performed in a transblot semi-dry setup using top (60 mM Tris, 40 mM CAPS, pH 9,6 + 0,1% SDS) and bottom buffer (60 mM Tris, 40 mM CAPS, pH 9,6 + 15% MeOH). Blocking was performed with 5% Elk-brand milk powder in TBS at 4˚C overnight. The membrane was then probed for an hour at RT with an anti-HIS-HRP antibody (Roche,1:1000 diluted) and chemiluminescence (LumiGlo, Cell Signalling) was detected using and X-Ray film (Fuji).

In vitro phosphorylation assay

The day before the *in vitro* phosphorylation assay was carried out, GST-fusion proteins were expressed and purified. Expression of GST-fusion proteins and lysate production was performed according to the method described for the pull-down assay. Proteins were purified using affinity chromatography with glutathione covered sepharose beads (resin) (Amersham) and all purification steps were conducted at 4ºC. 175µl of bead slurry were prepared by washing once with ice-cold PBS and centrifuged at 500g for 3 minutes followed by resuspension with 100µl of PBS and then loaded onto a drip column. The column was then equilibrated with extraction buffer (see pull-down protocol) for one hour after which the cell lysate (2ml) was loaded onto the column and sealed for incubation on a rocker table for one hour. The drip column was subsequently washed three times with PBS to remove unbound protein after which the sample was eluted with glutathione elution buffer (50 mM Tris-HCl, 10 mM Reduced Glutathione, pH 8.0). 10 µl samples were taken at each step for later analysis on SDS-PAGE. After purification, for the correct fractions, the protein concentration was determined using a BCA protein assay from Biorad according to the manufacturer's protocol. Approximately 1 µg of protein was used depending on its visibility after SDS-PAGE. Samples were incubated in a reaction buffer containing ^{32}P-γ-ATP (20 mM TRIS/HCL pH 7.5, 1 mM DTT, 15 mM $MgCl_2$, Magnesium solution: 1mM $MgCl_2$, ATP solution: 1 mM ATP, Radiolabeled ATP: 2 µCi ^{32}P-γ-ATP) in a total volume of 15 µl at 30°C for 30 minutes. After incubation, SDS sample buffer was added and samples were boiled for 5 minutes and separated using SDS-PAGE, (4% stack gel (60V), 7,5 – 12,5% polyacrylamide gel (120V)). After separation, the gel was Coomassie stained, and washed three times for 30 minutes using wash buffer (5% Trichloroacetic acid, 1% Sodium acid pyro phosphate). The gel was equilibrated for 5 minutes and 1 minute for the gel drying film using equilibration solution (40 % Methanol, 10% Glycerol, 7,5% acetic acid). Gel was dried using gel drying film and placed in a cassette with X- ray film and stored at -80°C for a period of 72 hours.

COP1 sequence alignment

COP1 sequences from species shown in Fig. 6 were obtained from phyotozome (http://www.phytozome.net) by blasting inferred proteomes with the AtCOP1 proteins sequence. COP1 sequences were then aligned with MEGA (http://www.megasoftware.net/) using a clustalW algorithm and manual corrections.

References

Abas, L., Benjamins, R., Malenica, N., Paciorek, T., Wiśniewska, J., Wirniewska, J., Moulinier-Anzola, J. C., Sieberer, T., Friml, J. and Luschnig, C. (2006). Intracellular trafficking and proteolysis of the *Arabidopsis* auxin-efflux facilitator PIN2 are involved in root gravitropism. *Nat. Cell Biol.* **8**, 249–56.

Baster, P., Robert, S., Kleine-Vehn, J., Vanneste, S., Kania, U., Grunewald, W., De Rybel, B., Beeckman, T. and Friml, J. (2012). SCF(TIR1/AFB)-auxin signalling regulates PIN vacuolar trafficking and auxin fluxes during root gravitropism. *EMBO J.* **32**, 260–274.

Bech-Otschir, D., Kraft, R., Huang, X., Henklein, P., Kapelari, B., Pollmann, C. and Dubiel, W. (2001). COP9 signalosome-specific phosphorylation targets p53 to degradation by the ubiquitin system. *EMBO J.* **20**, 1630–1639.

Benjamins, R., Quint, A., Weijers, D., Hooykaas, P. and Offringa, R. (2001). The PINOID protein kinase regulates organ development in *Arabidopsis* by enhancing polar auxin transport. *Development* **128**, 4057–67.

Benjamins, R., Galván, C. S., Hooykaas, P. J. J., Offringa, R., Galva, C. S., Hooykaas, P. J. J. and Offringa, R. (2003). PINOID-Mediated Signaling Involves Calcium-Binding Proteins. *Society* **132**, 1623–1630.

Bhalerao, R. P., Ekl??f, J., Ljung, K., Marchant, A., Bennett, M. and Sandberg, G. (2002). Shoot-derived auxin is essential for early lateral root emergence in Arabidopsis seedlings. *Plant J.* **29**, 325–332.

Chen, X., Yao, Q., Gao, X., Jiang, C., Harberd, N. P. and Fu, X. (2016). Shoot-to-Root Mobile Transcription Factor HY5 Coordinates Plant Carbon and Nitrogen Acquisition. *Curr. Biol.* **26**, 640–646.

Cluis, C. P., Mouchel, C. F. and Hardtke, C. S. (2004). The *Arabidopsis* transcription factor HY5 integrates light and hormone signaling pathways. *Plant J.* **38**, 332–347.

Crocco, C. D., Holm, M., Yanovsky, M. J. and Botto, J. F. (2010). AtBBX21 and COP1 genetically interact in the regulation of shade avoidance. *Plant J.* **64**, 551–562.

Davis, A. M., Hall, A., Millar, A. J., Darrah, C. and Davis, S. J. (2009). Protocol: Streamlined sub-protocols for floral-dip transformation and selection of transformants in *Arabidopsis thaliana*. *Plant Methods* **5**, 3.

Deng, X., Deng, X., Quail, P. H. and Quail, P. H. (1992). Genetic and phenotypic characterization of of cop1 mutants of Arabidopsis thaliana. *Plant J.* **2**, 83–95.

Dessau, M., Halimi, Y., Erez, T., Chomsky-Hecht, O., Chamovitz, D. a and Hirsch, J. a (2008). The *Arabidopsis* COP9 signalosome subunit 7 is a model PCI domain protein with subdomains involved in COP9 signalosome assembly. *Plant Cell* **20**, 2815–2834.

Dhonukshe, P., Huang, F., Galvan-Ampudia, C. S., Mähönen, A. P., Kleine-Vehn, J., Xu, J., Quint, A., Prasad, K., Friml, J., Scheres, B., et al. (2010). Plasma membrane-bound AGC3 kinases phosphorylate PIN auxin carriers at TPRXS(N/S) motifs to direct apical PIN recycling. *Development* **137**, 3245–55.

Ding, Z., Galván-Ampudia, C. S., Demarsy, E., Langowski, L., Kleine-Vehn, J., Fan, Y., Morita, M. T., Tasaka, M., Fankhauser, C., Offringa, R., et al. (2011). Light-mediated polarization of the PIN3 auxin transporter for the phototropic response in *Arabidopsis*. *Nat. Cell Biol.* **13**, 447–52.

Friml, J., Yang, X., Michniewicz, M., Weijers, D., Quint, A., Tietz, O., Benjamins, R., Ouwerkerk, P. B. F., Ljung, K., Sandberg, G., et al. (2004). A PINOID-dependent binary switch in apical-basal PIN polar targeting directs auxin efflux. *Science* **306**, 862–5.

Geldner, N., Dénervaud-Tendon, V., Hyman, D. L., Mayer, U., Stierhof, Y. D. and Chory, J. (2009). Rapid, combinatorial analysis of membrane compartments in intact plants with a multicolor marker set. *Plant J.* **59**, 169–178.

Gietz, D., St Jean, A., Woods, R. a and Schiestl, R. H. (1992). Improved method for high efficiency transformation of intact yeast cells. *Nucl Acid Res* **20**, 1425.

Gleave, A. P. (1992). A versatile binary vector system with a T-DNA organisational structure conducive to efficient integration of cloned DNA into the plant genome. *Plant Mol. Biol.* **38**, 455–1207.

Grefen, C., Donald, N., Hashimoto, K., Kudla, J., Schumacher, K. and Blatt, M. R. (2010). A ubiquitin-10 promoter-based vector set for fluorescent protein tagging facilitates temporal stability and native protein distribution in transient and stable expression studies. *Plant J.* **64**, 355–65.

Habets, M. E. J. and Offringa, R. (2014). PIN-driven polar auxin transport in plant developmental plasticity: A key target for environmental and endogenous signals. *New Phytol.* **203**, 362–377.

Hayes, S., Velanis, C. N., Jenkins, G. I. and Franklin, K. a. (2014). UV-B detected by the UVR8 photoreceptor antagonizes auxin signaling and plant shade avoidance. *Proc. Natl. Acad. Sci. U. S. A.* **111**, 11894–9.

Huang, F., Kemel Zago, M., Abas, L., van Marion, A., Galván Ampudia, C. S. and Offringa, R. (2010). Phosphorylation of Conserved PIN Motifs Directs *Arabidopsis* PIN1 Polarity and Auxin Transport. *Plant Cell* **22**, 1129–1142.

James, P., Halladay, J. and Craig, E. A. (1996). Genomic libraries and a host strain designed for highly efficient two-hybrid selection in yeast. *Genetics* **144**, 1425–1436.

Jang, S., Marchal, V., Panigrahi, K. C. S., Wenkel, S., Soppe, W., Deng, X.-W., Valverde, F. and Coupland, G. (2008). Arabidopsis COP1 shapes the temporal pattern of CO accumulation conferring a photoperiodic flowering response. *EMBO J.* **27**, 1277–88.

Karniol, B., Malec, P. and Chamovitz, D. a (1999). Arabidopsis FUSCA5 encodes a novel phosphoprotein that is a component of the COP9 complex. *Plant Cell* **11**, 839–848.

Keuskamp, D. H., Pollmann, S., Voesenek, L. A. C. J., Peeters, A. J. M. and Pierik, R. (2010). Auxin transport through PIN-FORMED 3 (PIN3) controls shade avoidance and fitness during competition. *Pnas* **3**, 22740–4.

Kircher, S. and Schopfer, P. (2012). Photosynthetic sucrose acts as cotyledon-derived long-distance signal to control root growth during early seedling development in Arabidopsis. *Proc. Natl. Acad. Sci.* **109**, 11217–11221.

Kleine-Vehn, J., Leitner, J., Zwiewka, M., Sauer, M., Abas, L., Luschnig, C. and Friml, J. (2008). Differential degradation of PIN2 auxin efflux carrier by retromer-dependent vacuolar targeting. *Proc. Natl. Acad. Sci. U. S. A.* **105**, 17812–7.

Lau, O. S. and Deng, X. W. (2012). The photomorphogenic repressors COP1 and DET1: 20 years later. *Trends Plant Sci.* **17**, 584–93.

Laubinger, S., Fittinghoff, K. and Hoecker, U. (2004). The SPA Quartet : A Family of WD-Repeat Proteins with a Central Role in Suppression of Photomorphogenesis in *Arabidopsis*. *Plant Cell* **16**, 2293–2306.

Laxmi, A., Pan, J., Morsy, M. and Chen, R. (2008). Light plays an essential role in intracellular distribution of auxin efflux carrier PIN2 in *Arabidopsis* thaliana. *PLoS One* **3**, e1510.

Lee, J., He, K., Stolc, V., Lee, H., Figueroa, P., Gao, Y., Tongprasit, W., Zhao, H., Lee, I. and Deng, X. W. (2007). Analysis of transcription factor HY5 genomic binding sites revealed its hierarchical role in light regulation of development. *Plant Cell* **19**, 731–49.

Leitner, J., Petrasek, J., Tomanov, K., Retzer, K., Parezova, M., Korbei, B., Bachmair, A., Zazimalova, E. and Luschnig, C. (2012). Lysine63-linked ubiquitylation of PIN2 auxin carrier protein governs hormonally controlled adaptation of *Arabidopsis* root growth. *Proc. Natl. Acad. Sci.* **109**, 8322–8327.

Maraschin, S. (2009). Protein ubiquitination in auxin signaling and transport. *Dr. Thesis https//openaccess.leidenuniv.nl/handle/1887/13868*.

Marhavý, P., Bielach, A., Abas, L., Abuzeineh, A., Duclercq, J., Tanaka, H., Pařezová, M., Petrášek, J., Friml, J., Kleine-Vehn, J., et al. (2011). Cytokinin modulates endocytic trafficking of PIN1 auxin efflux carrier to control plant organogenesis. *Dev. Cell* **21**, 796–804.

McNellis, T. W., von Arnim, a G. and Deng, X. W. (1994). Overexpression of *Arabidopsis* COP1 results in partial suppression of light-mediated development: evidence for a light-inactivable repressor of photomorphogenesis. *Plant Cell* **6**, 1391–1400.

Meijer, A. H., Schouten, J., Ouwerkerk, P. B. F. and Hoge, J. H. C. (2000). Yeast as Versatile Tool in Transcription Factor Research. In *Plant Molecular Biology Manual* (ed. Gelvin, S. B.) and Schilperoort, R. A.), pp. 29–57. Dordrecht: Springer Netherlands.

Nezames, C. D. and Deng, X.-W. (2012). The COP9 Signalosome: Its Regulation of Cullin-based E3 Ubiquitin Ligases and Role in Photomorphogenesis. *Plant Physiol.* **160**, 38–46.

Petrásek, J., Mravec, J., Bouchard, R., Blakeslee, J. J., Abas, M., Seifertová, D., Wisniewska, J., Tadele, Z., Kubes, M., Covanová, M., et al. (2006). PIN proteins perform a rate-limiting function in cellular auxin efflux. *Science* **312**, 914–8.

Preuten, T., Hohm, T., Bergmann, S. and Fankhauser, C. (2013). Defining the site of light perception and initiation of phototropism in *Arabidopsis*. *Curr. Biol.* **23**, 1934–8.

Sassi, M., Lu, Y., Zhang, Y., Wang, J., Dhonukshe, P., Blilou, I., Dai, M., Li, J., Gong, X., Jaillais, Y., et al. (2012). COP1 mediates the coordination of root and shoot growth by light through modulation of PIN1- and PIN2-dependent auxin transport in Arabidopsis. *Development* **139**, 3402–12.

Sawano, a and Miyawaki, a (2000). Directed evolution of green fluorescent protein by a new versatile PCR strategy for site-directed and semi-random mutagenesis. *Nucleic Acids Res.* **28**, E78.

Schirawski, J., Planchais, S. and Haenni, A. L. (2000). An improved protocol for the preparation of protoplasts from an established Arabidopsis thaliana cell suspension culture and infection with RNA of turnip yellow mosaic tymovirus: a simple and reliable method. *J. Virol. Methods* **86**, 85–94.

Serino, G., Su, H., Peng, Z., Tsuge, T., Wei, N., Gu, H. and Deng, X. W. (2003). Characterization of the last subunit of the Arabidopsis COP9 signalosome: implications for the overall structure and origin of the complex. *Plant Cell* **15**, 719–731.

Sheerin, D. J., Menon, C., zur Oven-Krockhaus, S., Enderle, B., Zhu, L., Johnen, P., Schleifenbaum, F., Stierhof, Y.-D., Huq, E. and Hiltbrunner, A. (2015). Light-activated phytochrome A and B interact with members of the SPA family to promote photomorphogenesis in Arabidopsis by reorganizing the COP1/SPA complex. *Plant Cell* **27**, 189–201.

Sibout, R., Sukumar, P., Hettiarachchi, C., Holm, M., Muday, G. K. and Hardtke, C. S. (2006). Opposite root growth phenotypes of hy5 versus hy5 hyh mutants correlate with increased constitutive auxin signaling. *PLoS Genet.* **2**, e202.

Skirpan, A., Wu, X. and McSteen, P. (2008). Genetic and physical interaction suggest that BARREN STALK 1 is a target of BARREN INFLORESCENCE2 in maize inflorescence development. *Plant J.* **55**, 787–97.

Uhle, S., Medalia, O., Waldron, R., Dumdey, R., Henklein, P., Bech-Otschir, D., Huang, X., Berse, M., Sperling, J., Schade, R., et al. (2003). Protein kinase CK2 and protein kinase D are associated with the COP9 signalosome. *EMBO J.* **22**, 1302–12.

Van Buskirk, E. K., Decker, P. V. and Chen, M. (2012). Photobodies in Light Signaling. *Plant Physiol.* **158**, 52–60.

Wei, N., Serino, G. and Deng, X.-W. (2008). The COP9 signalosome: more than a protease. *Trends Biochem. Sci.* **33**, 592–600.

Wisniewska, J., Xu, J., Seifertova, D., Brewer, P. B., Ru, K., Scheres, B., Blilou, I., Rouquie, D., Benková, E. and Friml, J. (2006). Polar PIN localization directs duxin flow in plants. *Science (80-.).* **312**, 833.

Yin, R., Arongaus, A. B., Binkert, M. and Ulm, R. (2015). Two distinct domains of the UVR8 photoreceptor interact with COP1 to initiate UV-B signaling in *Arabidopsis*. *Plant Cell* **27**, 202–13.

Zhang, K.-X., Xu, H.-H., Yuan, T.-T., Zhang, L. and Lu, Y.-T. (2013). Blue-light-induced PIN3 polarization for root negative phototropic response in *Arabidopsis*. *Plant J.* **76**, 308–321.

Zhu, L., Bu, Q., Xu, X., Paik, I., Huang, X., Hoecker, U., Deng, X. W. and Huq, E. (2015). CUL4 forms an E3 ligase with COP1 and SPA to promote light-induced degradation of PIF1. *Nat. Commun.* **6**, 7245.

Supplemental data

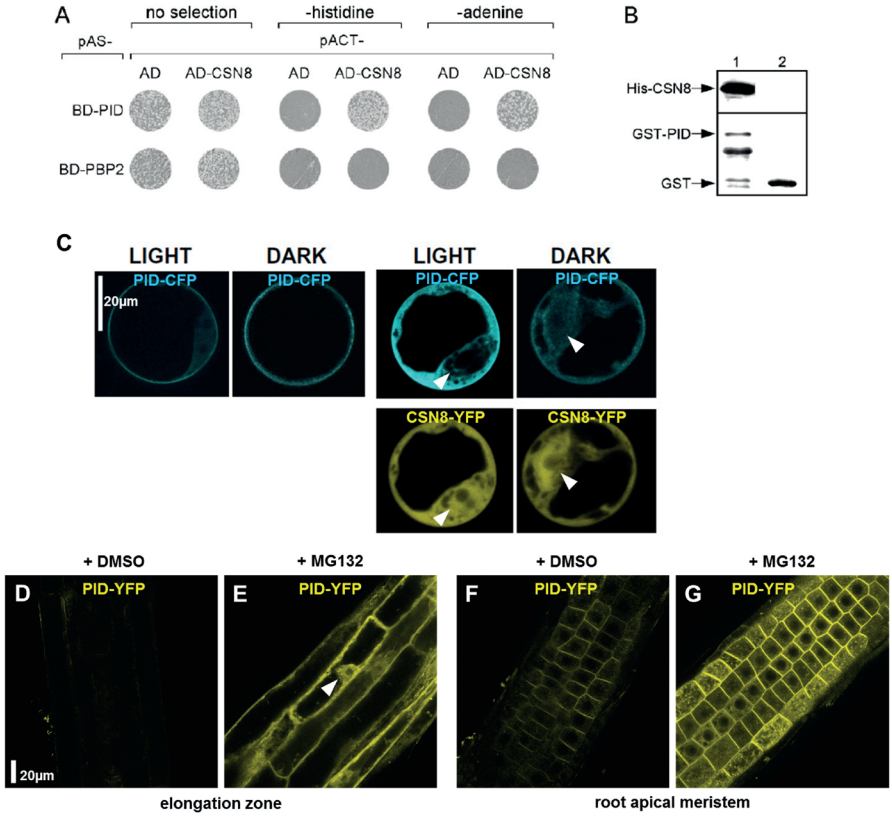

Figure S1: PID interacts with CSN8 in a yeast-two-hybrid and *in vitro* pull down assay and CSN8-YFP co-transfection and MG132 treatment results in nuclear PID.

(A) Yeast-two-hybrid assay with PID and PBP2 fused to the GAL4 binding domain (BD; pAS2.1 vector), and CSN8/COP9 fused to the GAL4 activation domain (AD) or the AD alone (pACT2 vector) in nonselective medium or in medium lacking either histidine or adenine. (B) In vitro pull-down of His-tagged CSN8/COP9 with GST-tagged PID (lane 1) and or with GST (lane 2) followed by immunodetection with anti-His antibodies (top panel). The coomassie-stained gel is shown in the bottom panel. (C) Confocal images of representative Arabidopsis protoplasts transformed with *35S::PID-CFP* alone (left two images) or co-transfected with *35S::CSN8-YFP* (right four images). Sixteen hours following transfection, cells were kept in continuous dark or transferred to light 4 hours before imaging. In the dark CSN8 sequesters PID to the nucleus (white arrows) and away from the plasma membrane. All images are to the same scale. (D-G) Confocal images of five day old *pid-14 PID::PID-YFP* seedlings treated with 50 µg MG132 or with DMSO as a control. (D) Control and (E) treatment of the elongation zone epidermis of the main root, the white arrow shows nuclear localization. (F) Control and (G) treatment of the main root meristem epidermis. All images are to the same scale.

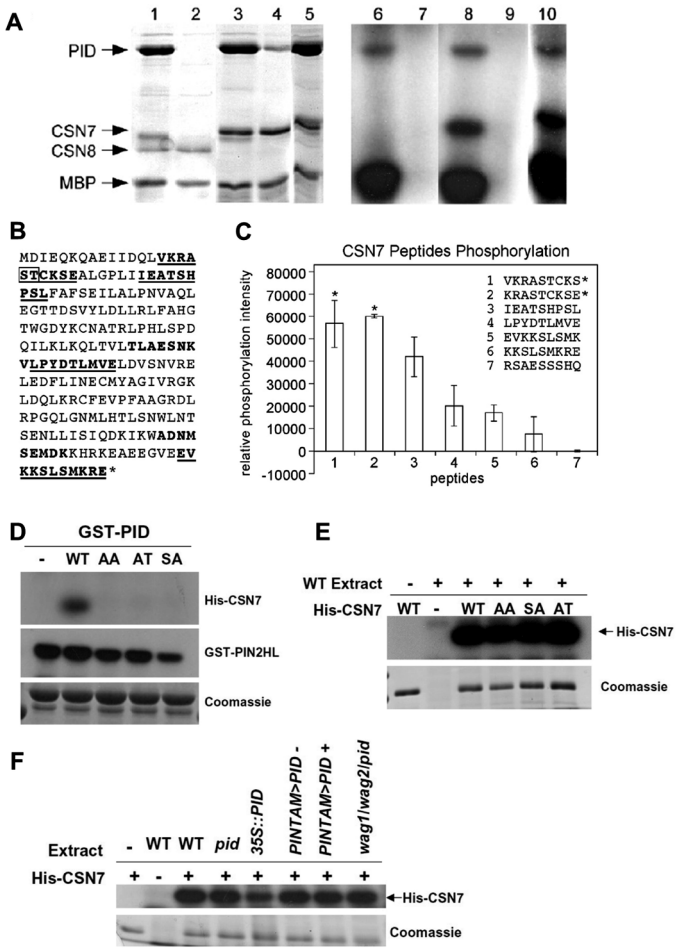

Figure S2: PID phosphorylates CSN7 in vitro, but does not contribute to the overall CSN7 phosphorylating activity in total protein extracts from Arabidopsis.

(A) Autoradiograph (right panel) and coomassie-stained gel (left panel) of in vitro phosphorylation assay using MBP (all lanes), His-CSN8 (lanes 1, 2, 5, 6, 7 and 10) and His-CSN7 (lanes 3, 4, 5, 8, 9 and 10) as substrates and PID (lanes 1, 3, 5, 6, 8 and 10) as protein kinase. (B) Amino acid sequence of CSN7, with all the putative phosphorylation sites identified by NetPhos as central residues within nine amino acid peptides indicated in bold. The peptides tested in the in vitro phosphorylation assay (C) are underlined and the putative PID phosphorylation sites are boxed in (B). BDL-derived peptide RSAESSSHQ (7) was used as a negative control. (D) *In vitro* phosphorylation assay showing the autoradiographs of GST-PIN2HL (positive control, all lanes), and His-CSN7-WT, -AA, -AT or –SA, incubated with GST-PID. The bottom panel depicts the coomassie stained gel. (E) Autoradiograph (upper panel) and coomassie-stained gel (lower panel) of an in vitro phosphorylation assay in which His-CSN7-WT, -AA, AT or –SA were incubated with 2 µg of total protein extract from Arabidopsis seedlings. (F) Autoradiograph (upper panel) and coomassie-stained gel (lower panel) of an in vitro phosphorylation assay in which 2 µg WT His-CSN7 was incubated with 2 µg of total protein extract of Arabidopsis wild type seedlings (WT), or seedlings from the *pid-14* loss-of function mutant, the *35S::PID line #21*(Benjamins et al., 2001), the tamoxifen-inducible PID line treated for 8h with DMSO (PINTAM>PID-), or with 2 µM tamoxifen (PINTAM>PID +), or the pid wag1 wag2 triple loss-of-function mutant.

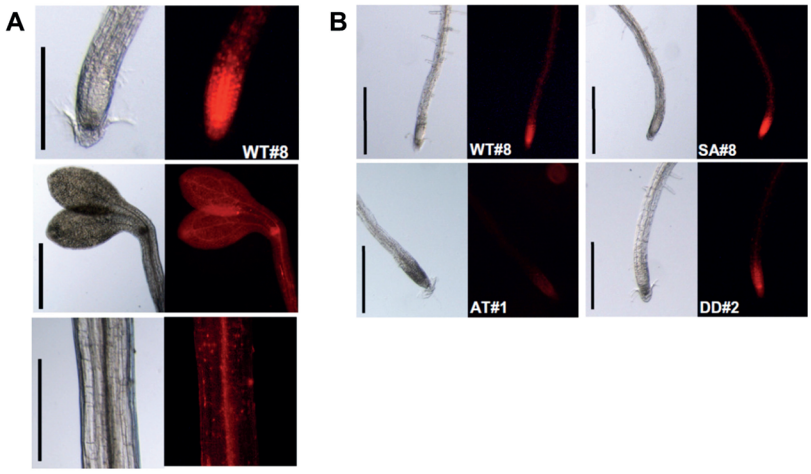

Figure S3: Expression pattern of *CSN7::CSN7-RFP* transformants.
(A) Epifluorescence microscopy of 7-day old etiolated seedlings showing the expression pattern of the complementing construct pCSN7::CSN7-mRFP in the cop15-1 mutant background. **(B)** Comparison of expression patterns among the wild type and the ST to SA, AT or DD versions of the pCSN7::CSN7-mRFP construct. Etiolated homozygous plants of the T3 generation were imaged at 7 dag. The scale bar represents 0.2 cm in **A** and 0.5 cm in **B**.

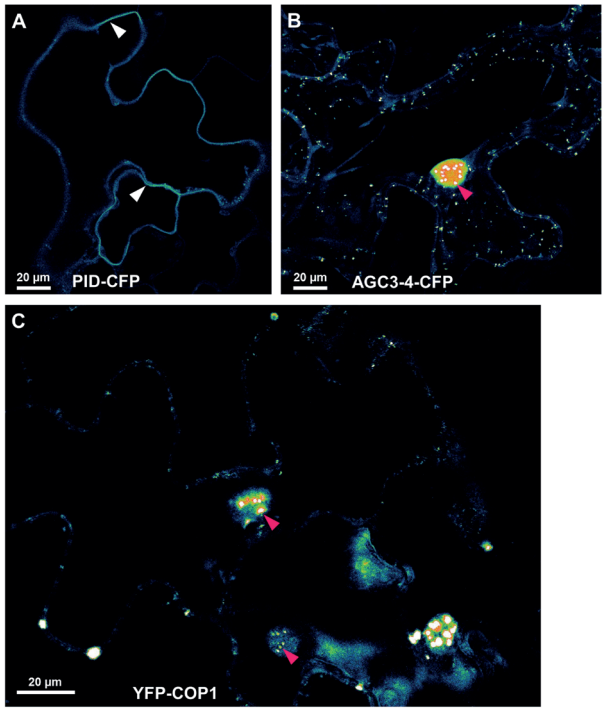

Figure S4: PID, AGC3-4 and COP1 localization in *N. tabacum* leaf epidermis.
Confocal images of *N. tabacum* leaf epidermis cells transiently transformed with an agrobacterium-borne constructs. (A) *35S::PID-CFP*, (B) *35S::AGC3-4-CFP,* (C) *UBQ::YFP-COP1*. Note the plasma membrane localization

(white arrow), nuclear spots (pink arrow) and cytoplasmic spots (green arrow).

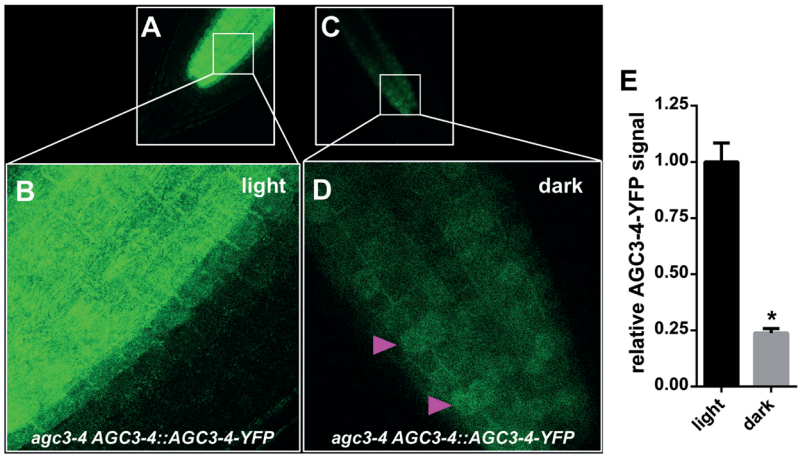

Figure S5: AGC3-4-YFP signal decreases in darkness.
(A) Representative picture of light-treated *agc3-4 AGC3-4::AGC3-4-YFP* seedlings (Chapter 3), showing AGC3-4-YFP signal in the root meristem (B shows detail of A). (C) *agc3-4 AGC3-4::AGC3-4-YFP* seedlings kept in the dark for three hours (pink arrows point to nucleus). (E) AGC3-4-YFP signal intensity was quantified in at least 8 seedlings per treatment using ImageJ. The values plotted are relative to the signal in light (Error bars indicate SEM, * = statistically significant p<0,001 using t-test.)

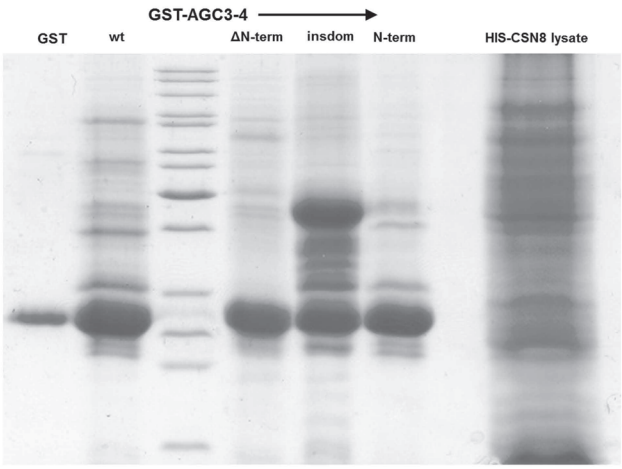

Figure S6: Original coomassie staining Figure 4C.
Coomassie stained gel of i*n vitro* pull-down of HIS-tagged CSN8 by GST-tagged PID and mutant versions thereof: Δinsdom = AGC3 insertion domain deleted, CAD = kinase domain without N- and C-terminal domains, ΔN-/C-term = deleted N-/C-terminal and ΔNtermΔCterm = both domains deleted, (for domain details, see methods)). A GST-only reaction and HIS-CSN8 lysate were loaded on the SDS-PAGE.

Table S1: Primers used in this study.

Primer name	Target gene	sequence	remarks
LB1 (SAIL)	N/A	GCCTTTTCAGAAATGGATAAATAGCCTTGCTTCC	left border primer SAIL
SALK LB primer	N/A	CGTCAAGCTCTAAATCGGGG	Custom left border primer SALK
P745	N/A	AACGTCCGCAATGTGTTATTAAGTTGTC	WiscDslox left border primer
SALK137391 FW	At2g32950	AAAACTTCAGCTCGGCATGT	*cop1* SALK137391 genotyping FW+BP = insert
SALK137391 rev	At2g32950	TCGAGCTGTCAATCCAGATG	*cop1* SALK137391 genotyping
SALK027212 FW	At2g32950	GCTTTATGCTTTGCCTGGAC	*cop1* SALK027212 genotyping FW+BP = insert
SALK027212 rev	At2g32950	TGTCCAGTTTCGTTTGTTTCC	*cop1* SALK027212 genotyping
HY5 N679707 LP		TTCACTCTCGATATCCGTTCG	*hy5* SALK056405 genotyping
HY5 N679707 RP		ATGCGAGTGAATGACCATTTC	*hy5* SALK056405 genotyping RP+BP = insert
HYH wisclox LP		ACCCACACGCTCTGTGAATAC	*hyh* WiscDsLox253D10 genotyping
HYH wisclox RP		ACTCGCATAAGAACATGTGGG	*hyh* WiscDsLox253D10 genotyping RP+BP = insert
pid-14 LP	At2g34650	CAGTCGGGAAACTCAACTGTC	*pid-14* genotyping
pid-14 RP	At2g34650	ATTTTGCGATGAAAGTTGTGG	*pid-14* genotyping
PID attB F	At2g34650	GGGGACAAGTTTGTACAAAAAAGCAGGCTTCAGCATGTTACGAGAATCAGACGGT	*PID* gateway cloning
PID attB R -stop	At2g34650	GGGGACCACTTTGTACAAGAAAGCTGGGTCAAAGTAATCGAACGCCGCTGG	*PID* gateway cloning
AGC3-4 attB F	At2g26700	GGGGACAAGTTTGTACAAAAAAGCAGGCTTCAGCATGGCTAATTCTAGTATCTTT	*AGC3-4* gateway cloning
AGC3-4 attB R -stop	At2g26700	GGGGACCACTTTGTACAAGAAAGCTGGGTCAAAATAATCAAAATAATTAGA	*AGC3-4* gateway cloning
CSN8 attB F	At4g14110	GGGGACAAGTTTGTACAAAAAAGCAGGCTGGATGGATCTTTCGCCTGTT	*CSN8* cloning primer
CSN8 attB R	At4g14110	GGGGACCACTTTGTACAAGAAAGCTGGGTCATGTTCAAGGTGGAACAC	*CSN8* cloning primer
CSN7 attB F	At1g02090	ACGCAAGTCGACAAGATGGATATCGAGCAGAAGCAAGC	*CSN7* cloning primer
CSN7 attB R	At1g02090	GATAGATCTAACAGAGGATCTTATACAAGTTG	*CSN7* cloning primer
COP1 attB F	At2g32950	GGGGACAAGTTTGTACAAAAAAGCAGGCTGGATGGAAGAGATTTCGACG	*COP1* cloning primer
COP1 attB R	At2g32950	GGGGACCACTTTGTACAAGAAAGCTGGGTCCGCAGCGAGTACCAGAAC	*COP1* cloning primer
csn7ST-ATF	At1g02090	GCTCGTGAAGCGAGCTTCTAGGTGCAAATCCGAGGC	Site directed ST>AT mutation
csn7ST-ATR	At1g02090	GCCTCGGATTTGCACCTAGAAGCTCGCTTCACGAGC	Site directed ST>AT mutation
csn7ST-SAF	At1g02090	GCTCGTGAAGCGAGCTAGGACTTGCAAATCCGAGGC	Site directed ST>SA mutation
csn7ST-SAR	At1g02090	GCCTCGGATTTGCAAGTCCTAGCTCGCTTCACGAGC	Site directed ST>SA mutation
csn7ST-DDF	At1g02090	GCTCGTGAAGCGAGCTGATGATTGCAAATCCGAGGC	Site directed ST>DD mutation
csn7ST-DDR	At1g02090	GCCTCGGATTTGCAATCATCAGCTCGCTTCACGAGC	Site directed ST>DD mutation

Primer name	Target genesequence		remarks
COP1 S->A mutagenesis NheI	At2g32950	ACCTGACCCGCGAACAGCTAGCGTTGGTGAAG	Site directed mutagenesis primer 5′ phosphorylated
COP1 S->E AvaII	At2g32950	CCTGACCCGAGGACCGAATCAGTTGGTG	Site directed mutagenesis primer 5′ phosphorylated
attB SV40-PID S		GGGGACAAGTTTGTACAAAAAAGCAGGCTTCATGCCTAAGAAGAAGAG-GAAGGTTGGATTACGAGAATCAGACGGTGAG	forward Gateway primer to construct SV40-PID in combination with 'PID attB R –stop' primer
pDONR207 F	N/A	TCTTCCGACTGAGCCTTT	entry vector primer
pDONR207 R	N/A	AGCTGGATGGCAAATAATGA	entry vector primer
35S F	N/A	CGCACAATCCCACTATC	35S promoter primer
pART27 F	N/A	GAGCGGATAACAATTTCACACAG	Destination vector
pUNI51 rev	N/A	AGAAGGCACAGTCGAGG	pUNI colony PCR primer
pGEX-KG seq Fw	N/A	GGTATGGCTGTGCAGGTCGT	pGEX cloning primer
AGC3-4 actseg FWattb	At2g26700	GGGGACAAGTTTGTACAAAAAAGCAGGCTTAATGCTCTCAGATTTCGATCTCT	*AGC3-4* insertion domain cloning primer
AGC3-4 actseg Revattb	At2g26700	GGGGACCACTTTGTACAAGAAAGCTGGGTCTTCGGGTGCCAAGTACTCATGTG	*AGC3-4* insertion domain cloning primer
AGC3-4 N-tail FWattb	At2g26700	GGGGACAAGTTTGTACAAAAAAGCAGGCTTAATGGCTAATTCTAGTATCTTTT	*AGC3-4* N-terminal domain cloning primer
AGC3-4 N-tail Revattb	At2g26700	GGGGACCACTTTGTACAAGAAAGCTGGGTTTCCGATGTCACCACTTCCCAACC	*AGC3-4* N-terminal domain cloning primer
AGC3-4 -N-tail FWattb	At2g26700	GGGGACAAGTTTGTACAAAAAAGCAGGCTTAATGAGTGTGTACCTCTGCCAAA	*AGC3-4* ΔN-terminal domain cloning primer
AGC3-4 -N-tail Revattb	At2g26700	GGGGACCACTTTGTACAAGAAAGCTGGGTAAAAATAATCAAAATAATTAGACA	*AGC3-4* ΔN-terminal domain cloning primer